Comparison of semiclassical line-shape models to rovibrational H_2O spectra measured by frequency-stabilized cavity ring-down spectroscopy

Daniel Lisak,[1,2] Joseph T. Hodges,[1] and Roman Ciuryło[2]
[1]*Process Measurements Division, National Institute of Standards and Technology, 100 Bureau Drive, Gaithersburg, Maryland 20899, USA*
[2]*Instytut Fizyki, Uniwersytet Mikołaja Kopernika, ul. Grudziadzka 5/7, 87-100 Toruń, Poland*
(Received 9 November 2005; published 19 January 2006)

A single-mode cavity ring-down spectrometer, which incorporates a stabilized and tuneable comb of resonant frequencies and a continuous-wave external-cavity diode probe laser, was used to study rovibrational absorption line shapes within the $2\nu_1+\nu_3$ and $3\nu_3$ vibrational bands of water vapor. This spectrometer, which has a noise-equivalent absorption coefficient of 2×10^{-9} cm^{-1} Hz$^{-1/2}$ and frequency resolution of 50 kHz, enables high-precision measurements of line-shape effects and pressure shifting of relatively weak absorption transitions. We investigated the room-temperature pressure dependence over the range from 0.5 Pa to 50 kPa of two H_2 ^{16}O transitions perturbed by He, N_2, and SF_6. Foreign-gas broadening and pressure-shift coefficients were determined for a relatively strong transition at 10 687.36 cm^{-1}, and for a weaker transition at 10 834.34 cm^{-1} the self- and N_2-broadening and pressure-shift parameters were measured. In the low-pressure limit the room-temperature Doppler width was measured within 0.2% of its expected value. Doppler-free saturation effects were also observed with linewidths below 2 MHz. The data were compared to semiclassical line-shape models that considered the influence of Dicke narrowing as well as the speed dependence of pressure broadening and pressure shifting. Taking both of these effects into account gave the best agreement with our observations and allowed us to model the observed asymmetries of experimental profiles. Hard- and soft-collision as well as billiard-ball collision models were considered. These results allowed us to quantify systematic errors in line intensity and in pressure broadening associated with oversimplified models of line shape.

DOI: 10.1103/PhysRevA.73.012507 PACS number(s): 33.20.−t, 33.70.Jg, 33.70.Fd, 42.62.Fi

I. INTRODUCTION

A fundamental understanding of absorption line shapes of atomic and molecular absorption is required to determine line intensities and transition frequencies from absorption spectra. The same is also valid for Raman spectroscopy [1]. Line shapes depend on the motion of the absorber with respect to the propagation direction of the incident light and on collisional interactions between the absorbing species (in the upper and lower states) and perturbing partners. Many models have been developed yielding a number of testable theoretical line shapes, with each model being valid to a certain level of approximation depending upon the underlying assumptions. Thus any measurement of line intensity is likely to be no more accurate than the line-shape model which is used to fit the observed spectrum. Such considerations are relevant to a variety of applications in which absorber concentrations are determined from quantitative spectroscopic methods [2–5]. For example, once line intensities have been assigned from primary measurements, absorber concentration can be determined from absorption spectra of previously characterized transitions. It follows that, with regard to such spectroscopic concentration measurements, any uncertainty in line intensity originating from line-shape errors introduces a corresponding systematic uncertainty in absorber concentration. Another application where line intensities and knowledge of line shapes plays a crucial role is that of spectroscopic temperature measurements that are based on the comparison of line intensities [6–9]. Finally accurate intensity measurements are key to addressing some fundamental problems like the dependence of line intensity on the perturber gas pressure. This dependence, besides a relatively well-understood line-mixing effect [10,11], could be caused by the formation of van der Waals complexes or the failure of the impact approximation [12].

In this article, we use cavity ring-down spectroscopy (CRDS) for high-precision line-shape measurements of water vapor, a primary goal being the quantification of systematic uncertainties in the measurement of line intensities associated with overly simplistic line-shape models. In CRDS the passive decay time of light intensity from an optical resonator is measured. This decay time is directly related to the total base losses of the optical resonator plus the absorption losses in the cavity medium [13,14]. Attractive properties of CRDS include its relatively low detection limits, compact sample volumes, and potentially high spectral resolution. The minimum detectable change in the absorption coefficient α_{min} is typically $<1\times10^{-8}$ cm^{-1}, and ring-down cells generally occupy <1 m in length. The compact nature of CRDS systems is a distinct advantage over other high-sensitivity methods such as direct laser absorption and Fourier transform spectroscopy which require relatively bulky and long multipass sample cell geometries. With regard to spectral resolution, the vast majority of CRDS experiments have used relatively broadband pulsed lasers where the laser bandwidth generally cannot be neglected relative to the linewidth of the absorption transition [15]. Even for excitation by continuous wave (cw) single-mode lasers, [16–18] nonlinearities in fre-

TABLE I. Summary of water vapor transitions considered here. Intensity based on $T=296$ K. $[V,Q]'$ and $[V,Q]''$ correspond to upper and lower (vibrational V, rotational Q) states, respectively. Data and quantum assignments from HITRAN 2004 [24].

Transition	$\tilde{\nu}_0$ [cm^{-1}]	Intensity [cm^2 cm^{-1} molecule^{-1}]	V'	V''	Q'	Q''
A	10687.36209	6.45×10^{-22}	201	000	404	303
B	10834.34703	1.94×10^{-25}	003	000	515	532

quency tuning can complicate the interpretation of ring-down spectra, potentially leading to distortions of the intrinsic line-shape of individual transitions. Specifically, narrowband CW lasers with linewidths near 1 MHz have gained popularity among practitioners of CRDS. However, these cw-CRDS approaches usually do not fully exploit the spectral resolution commensurate with the kHz-level linewidths of ring-down cavities. Typically the ring-down cavity length is modulated to bring the local cavity mode into resonance with the laser frequency and the laser frequency detuning is determined through independent measurements [19,20]. Increased data rates in cw-CRDS can be obtained by either locking the probe laser to the ring-down cavity or, vice versa, in conjunction with an external étalon to measure the frequency tuning of the probe laser [21]. Nevertheless, nonlinearities in the $PbZr_xTi_yO_3(pzt)$ devices used to length tune either the probe laser frequency, the ring-down cavity mirrors, or the length of an external étalon typically yield a spectral resolution no better than 5 MHz. We show in this article, however, that these limitations of CRDS can be overcome using the frequency-stabilized ring-down cavity technique, thus paving the way for high-precision line-shape studies on relatively weakly absorbing systems.

The remainder of the article is organized as follows. A description of the experimental apparatus and measurement technique is given, followed by a discussion of the physical origin of line-shape effects. We present line-shape measurements acquired with a frequency-stabilized CRDS apparatus. Two rovibrational absorption transitions of $H_2{}^{16}O$ having intensities differing by more than three orders of magnitude are considered. The respective transition wave numbers $\tilde{\nu}_0$, intensities, and vibrational and rotational assignments are given in Table I. The strong transition and the weak transition are arbitrarily labeled A and B, respectively. For transition A, we report line-shape measurements in the Doppler limit and in the domain of foreign-gas pressure broadening over the pressure range $p=6-53$ kPa for trace quantities of H_2O in He, N_2, and SF_6. We report measurements on transition B and consider both self-broadening and broadening by N_2.

II. EXPERIMENTAL TECHNIQUE

The measurements were taken using the frequency-stabilized ring-down spectrometer at the National Institute of Standards and Technology (NIST, in Gaithersburg, MD), described in Refs. [22,23]. As discussed in [23] spectral scans are automated using two servos, the first of which maintains resonance of the ring-down cavity length as the stabilized reference laser is frequency shifted using a variable-frequency acousto-optic modulator (AOM) and the second of which maintains a time-averaged lock of the external cavity diode laser (ECDL) frequency (used as the probe laser) to the local fundamental transverse mode of the ring-down cavity. To realize probe laser frequency shifts that exceed the tuning range of the AOM, the ECDL can be tuned and relocked to an adjacent longitudinal mode order of the cavity by rapidly tuning to the next ring-down cavity mode (and thus breaking the lock) and then waiting for the servo to recapture the probe laser lock to the ring-down cavity. This scanning approach yields a linear axis for frequency shifts that does not depend on the external étalon used to realize the probe laser frequency lock, but depends on (1) the stability of the reference laser to which the ring-down cavity is locked (0.35 MHz), (2) the standard uncertainty (0.15 MHz) in the cavity free spectral range (FSR), and (3) the small nonlinearity of the ring-down cavity frequency comb (less than 1 kHz) associated with the absorbing cavity medium [22]. See Eq. (6) of [22] for the expression relating probe laser detuning to system observables. Absolute frequencies of the probe laser beam were measured at the beginning of each spectrum with a commercial scanning Michelson-interferometer wavelength meter having a combined standard uncertainty of 60 MHz and resolution of 20 MHz.

We used ring-down mirrors with nominal transmission losses of 3.7×10^{-4}, approximately 10 times greater than those used previously in [23]. Consequently, ring-down signal acquisition rates f_{acq} increased to more than 100 Hz and peak ring-down signal intensities and base losses (inversely proportional to the empty-cavity ring-down time) were also increased with respect to previously reported values in Ref. [23]. The system noise-equivalent absorption coefficient, which is given by $\sqrt{2}\sigma_\alpha f_{\mathrm{acq}}^{-1/2}$ where σ_α is the absorption coefficient noise level, was approximately 2×10^{-9} cm^{-1} Hz$^{-1/2}$ for $f_{\mathrm{acq}}=100$ Hz. Except for the ring-down cavity mirrors and the addition of a 500-Ω termination resistance at the ring-down signal photoreceiver, all components of the present system are given in [23]. All ring-down signals were sampled at 25 Msamples s^{-1} and were stored to a computer disk for post-processing, and each time constant was determined using a Levenberg-Marquardt least-squares fit of a three-parameter (i.e., time constant, initial intensity, base-line offset) exponential decay model to the data. For each frequency step at least 300 ring-down decay signals were acquired and individually fit. The local spectral value for the cavity losses was then based upon the ensemble average of the fitted time constants. Except for the Doppler-free saturation feature discussed below the frequency step size was nominally 15 MHz, thus giving at least 60 points across the

full width at half maximum (FWHM) of each spectrum.

All measurements were made at room temperature, and the cell temperature was measured with a calibrated four-wire industrial-grade platinum resistance thermometer mounted in good thermal contact with a 12.5-mm-diam stainless steel tube connecting the ring-down mirror mounts. The gas temperature measurements were estimated to have a combined standard uncertainty of 0.05 K.

The pressure in the ring-down cavity was monitored with two capacitance diaphragm gauges having full scale ranges of 13.3 kPa and 133 kPa, respectively, and combined standard uncertainties of 13 Pa. The sample gases were introduced into the ring-down cavity through a gas manifold containing all-metal face seals, electropolished stainless-steel tubing, and high-purity isolation valves. Water vapor was introduced into the evacuated ring-down cell by momentarily opening a valve connected to a small reservoir of distilled and degassed liquid water.

To prepare for the acquisition of transition A spectra, we tuned the laser frequency to the absorption peak and continuously monitored the instantaneous water vapor concentration via the single-pass ring-down losses (mirror transmittance plus the gas phase absorbance). With the water vapor source isolated from the cell, we pumped on the ring-down cell until the absorption losses were approximately twice that of the empty-cavity losses. Based on the known line intensity for transition A, this concentration corresponded to a pressure of $\approx$0.5 Pa of water vapor. Next, the cell was backfilled to the desired pressure of buffer gas. The water vapor concentration increased with the introduction of the buffer gas, thus requiring additional pumping and reintroduction of water vapor and buffer gas until the water vapor concentration yielded an acceptable absorption level for the ring-down measurements.

Note that for transition A, the water vapor pressure in the cell invariably showed a tendency to drift upward in time because of outgassing effects from the internal surfaces of the ring-down cell. Typically, the system was allowed to equilibrate overnight, such that the drift rate was essentially linear in time and the fractional rate of change of water vapor concentration was $<10^{-2}$ h^{-1}. This drift in the background contributed a slight linear baseline to the spectra and was readily accounted for in all the measurements reported below. In the case of transition B, the partial pressure of water vapor was always $>$400 Pa and the initial charge of water vapor was measured directly with the low-range capacitance diaphragm pressure gauge. Unlike the situation with regard to transition A, no significant drift in the water vapor pressure was observed at the elevated pressures required for measurements on transition B.

In order to ensure that instrumental effects do not confound the measurements of line shape the following criteria should be met. First, the observed absorption losses (vertical axis) and frequency detuning (horizontal axis) must be free of instrumental nonlinearities that cause spectral distortion, and second, the measurements must resolve spectral features (associated with collisional narrowing and speed-dependent pressure-broadening and pressure-shifting phenomena) on a frequency scale much smaller than the transition Doppler width. With the goal of satisfying these criteria as system performance targets, we measured transition A in the low-

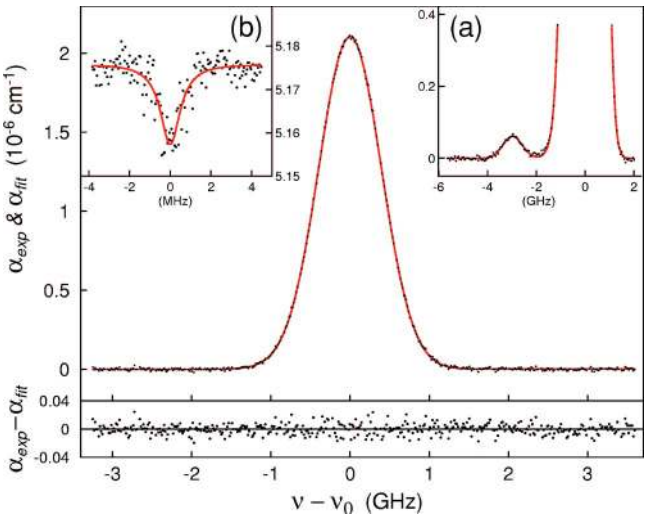

FIG. 1. (Color online) Absorption spectrum of transition A at the low-pressure limit and a least-squares Gaussian fit to the measurements: (a) weak transition close to transition A measured at $p=7\times10^{-3}$ kPa and (b) Lamb dip observed at the line center.

pressure limit for which the line shape was expected to be a Doppler profile. Figure 1 gives the observed absorption spectrum and a least-squares fit to the measurements. Close examination of the measurements revealed a weak water vapor absorption transition centered at a frequency detuning of ≈-3 GHz, where detuning=0 corresponds to line center of transition A. This weak line is consistent with the HITRAN 2004 line list [24]. This version of HITRAN also specifies another weak transition occurring at a frequency detuning of -1.3 GHz, which is only slightly more than one Doppler FWHM from the peak of transition A and thus difficult to resolve. According to HITRAN the relative line intensities of these two weak lines are 0.38% and 0.56% of the line intensity of line A. It was necessary to make a separate scan at higher water vapor concentration in order to improve the signal-to-noise ratio (SNR) of the observed spectral feature at -3 GHz. These data and associated Gaussian fits, given in inset (a) of Fig. 1, yielded precise measures of the detuning and intensity of the weak transition relative to those of transition A. With these constraints and using the HITRAN 2004 values for the detuning and relative intensity of the transition at -1.3 GHz, we fit the sum of three Gaussian line shapes to the measured profile given in Fig. 1. The result is a best-fit Doppler width for transition A of 929.5(14) MHz (FWHM) which can be compared to the expected value of 929.90(8) MHz based on the measured cell temperature of 295.81(5) K. These measured and expected Doppler widths agree to within their combined uncertainties, and importantly, inspection of the fit residuals reveals that, within the noise level of the measurements, no systematic distortion of the profile was observed.

To quantify the spectral resolution of the frequency-stabilized CRDS technique, we probed transition A in frequency steps of 50 kHz searching for a Doppler-free saturation dip occurring at the line center [25,26]. See inset (b) of Fig. 1 in which an intensity-dependent saturation dip with a FWHM $\simeq$1.3 MHz was clearly resolved. These results illus-

trate that the spectral resolution is <100 kHz, an upper bound well below the MHz-level intrinsic frequency jitter of the probe laser and approaching the $\simeq 50$ kHz FWHM linewidth of the ring-down cavity. The integrated area of the saturation dip is $<10^{-4}$ times the area of the dominant Doppler profile and therefore had minimal influence on measurement of the Doppler width of transition A. We note that saturation effects at the line center were manifest in nonexponential ring-down decay signals. However, a more detailed discussion of saturation effects in the frequency-stabilized CRDS apparatus is outside of the scope of this paper.

III. LINE-SHAPE MODELS

Rigorous models of the line shape of pressure- and Doppler-broadened lines which also take into account velocity-changing collisions of the absorber by the perturber require quantum-mechanical calculations [27–31]. Such calculations can be done when the interaction potentials between absorber and perturber are known for both the upper and lower states of absorber; however, they are rather complicated and so far they have been made only for D_2 lines perturbed by He [32]. Usually semiclassical line-shape models provide simple analytical formulas and these models are commonly used to analyze and fit experimental data. Reviews of these models can be found in Refs. [33–38]. Here we indicate only the basic assumptions and simplifications made in deriving the profiles that we used in our data analysis.

In analogy to the self-structure factor [39] used in statistical physics, the shape of an isolated spectral line can be written [31,40]

$$I(\omega) = \frac{1}{\pi} \mathrm{Re}(1, h(\omega;\vec{v})) \tag{1}$$

in terms of a complex function $h(\omega;\vec{v})$ which fulfills the kinetic equations

$$1 = -i(\omega - \omega_0 - \vec{k}\cdot\vec{v})h(\omega;\vec{v}) - \hat{S}^f h(\omega;\vec{v}), \tag{2}$$

where $\vec{v}$ is the absorber velocity, ω_0 is the resonance angular frequency, and ω and $\vec{k}$ are the angular frequency and wave vector of the light, respectively. The bracket $(a,b) = \int d^3\vec{v} f_m(\vec{v}) a^*(\vec{v}) b(\vec{v})$ denotes the scalar product of two functions $a(\vec{v})$ and $b(\vec{v})$ where $f_m(\vec{v}) = (\pi v_m)^{-3/2} \exp(-v^2/v_m^2)$ is the Maxwell velocity distribution, $v_m = \sqrt{2k_BT/m_A}$ is the most probable speed of the absorber, m_A is the mass of the absorber, k_B is the Boltzmann constant, and T is the temperature of the gas. Finally the collision operator $\hat{S}^f$ describes the influence of absorber collisions with perturbers on the line shape.

The collision operator $\hat{S}^f$ has a complicated structure; nevertheless, it is always formally possible to split this operator into two parts:

$$\hat{S}^f = \hat{S}^f_D + \hat{S}^f_{VCD}. \tag{3}$$

The first part is responsible for ordinary collisional broadening and shifting. It is called the dephasing collision operator:

$$\hat{S}^f_D = -\Gamma(v) - i\Delta(v), \tag{4}$$

where $\Gamma(v)$ and $\Delta(v)$ are the speed-dependent collisional width and collisional shift, respectively. This part is relatively easy to handle and can be determined using a wide variety of methods [41–45]. The remaining part $\hat{S}^f_{VCD}$ describes the joint effect of the velocity change and dephasing induced by collisions. Therefore this operator is called the velocity-changing and dephasing collision operator.

An important parameter describing the change of absorber velocity by collisions is the effective frequency of velocity-changing collisions $\nu_{\mathrm{diff}} = k_BT/(m_AD)$. This quantity is directly related to the mass diffusion coefficient D. Defining the velocity-changing collision operator $\hat{S}^f_{VC}$ which does not include any dephasing processes, we can approximate this frequency by the proper matrix element of this operator [39], $\nu^{(0)}_{\mathrm{diff}} = (\varphi_{01}(\vec{v}), \hat{S}^f_{VC}\varphi_{01}(\vec{v}))$, where

$$\varphi_{nl}(\vec{v}) = \sqrt{\frac{\pi^{1/2} n!(2l+1)}{2\Gamma(n+l+3/2)}} \left(\frac{v}{v_m}\right)^l L_n^{l+1/2}(v^2/v_m^2) P_l(\vec{e}_k\cdot\vec{e}_v) \tag{5}$$

are the basis functions in which the function $h(\omega,\vec{v})$ can be expanded. Here $\Gamma(\cdots)$ is the gamma-Euler function, $L_n^{l+1/2}(x^2)$ are the associated Laguerre polynomials, $x = v/v_m$ is the reduced absorber speed, $P_l(y)$ are Legendre polynomials, $y = \vec{e}_k\cdot\vec{e}_v$ is the cosine of the angle between the velocity vector $\vec{v} = v\vec{e}_v$ and the wave vector $\vec{k} = k\vec{e}_k$, and $\vec{e}_v$ and $\vec{e}_k$ are unit vectors. Using the frequency of collisions $\nu^{(0)}_{\mathrm{diff}}$ calculated in this way the first-order approximation $D^{(0)}$ of the diffusion coefficient can be found.

In analogy to the frequency ν_{diff} for operator $\hat{S}_{VC}$, an optical frequency of velocity-changing collisions ν_{opt} corresponding to the velocity-changing and dephasing collision operator $\hat{S}_{VCD}$ can be introduced. This optical frequency ν_{opt} can be complex valued in the general case. The optical frequency of the velocity-changing collisions can also be estimated in the first-order approximation:

$$\nu^{(0)}_{\mathrm{opt}} = (\varphi_{01}(\vec{v}), \hat{S}^f_{VCD}\varphi_{01}(\vec{v})). \tag{6}$$

In contrast to the dephasing collision operator, there is no easy way to correctly model the velocity-changing and dephasing collision operator [27,29,31]. Therefore to analyze experimental data we are forced to use a rather phenomenological approach to the problem. We will approximate the $\hat{S}^f_{\mathrm{VCD}}$ operator by simple models of velocity-changing collision operators $\hat{S}^f_{\mathrm{mod}}$ (like the soft-collision model [46,47], hard-collision model [48,49], or billiard-ball model [31,37,39])

$$\hat{S}^f_{\mathrm{VCD}} \approx \frac{\nu^{(0)}_{\mathrm{opt}}}{\nu^{(0)}_{\mathrm{mod}}} \hat{S}^f_{\mathrm{mod}}, \tag{7}$$

where $\nu^{(0)}_{\mathrm{mod}} = (\varphi_{01}(\vec{v}), \hat{S}^f_{\mathrm{mod}}\varphi_{01}(\vec{v}))$. To include the dephasing aspect of velocity-changing collisions in our treatment we allow the optical frequency of velocity-changing collisions

ν_{opt} to differ from ν_{diff} and to be complex if necessary. Following other authors [49–52] we use

$$\nu_{\mathrm{opt}}^{(0)} \approx \nu_{\mathrm{diff}} - \eta(\Gamma + i\Delta), \tag{8}$$

where η is a correlation coefficient and Γ and Δ are the collisional width and collisional shift averaged over the Maxwellian distribution of absorber speed, respectively. The problem of correlation between velocity-changing and dephasing collisions and its quantification was analyzed on both a semiclassical and a quantum basis [53–55].

The simplest model taking motion of the absorber into account assumes free motion on straight-line trajectories and a Maxwellian distribution of absorber velocity. In this simple case velocity-changing collisions are neglected. The additional assumption that the collisional (pressure) width and collisional shift are independent of absorber velocity leads to the well-known Voigt profile (VP). The dependence of collisional parameters on absorber velocity, characteristic of so-called speed-dependent effects, is particularly important in the case of high perturber-to-absorber mass ratios, a case in point being the H_2O-SF_6 system. The speed-dependent Voigt profile (SDVP) can be used in such a case to describe the line shape as was first done by Berman [41]. Application of this profile, however, requires knowledge of the dependence of collisional parameters on absorber velocity, which can be calculated from absorber-perturber interaction potentials. In most cases exact potentials are not known and approximate formulas are commonly used. When interaction potentials are approximated by an inverse power form $V(r)=C_q/r^q$, simple analytical formulas for the speed dependence of the collisional width and collisional shift exist [42]:

$$\frac{\Gamma(xv_m)}{\Gamma} = \frac{\Delta(xv_m)}{\Delta} = \left(1+\frac{m_P}{m_A}\right)^{-(q-3)/(2q-2)} M\left(-\frac{q-3}{2q-2}, \frac{2}{3}, -\frac{m_P}{m_A}x^2\right), \tag{9}$$

where m_P and m_A are masses of perturber and absorber, respectively, and $M(\ldots,\ldots,\ldots)$ denotes the confluent hypergeometric function. Speed-dependent effects may lead to line narrowing and asymmetry near the line center. It is worth noting that in order to model the line asymmetry associated with the speed-dependent effects one must know the pressure shift of the line.

For molecular infrared lines clear evidence of the influence of velocity-changing collisions on line shape has been observed in many cases. Collisional (Dicke) narrowing should occur when the mean free path of the absorber is shorter than the wavelength of the absorption transition. Two simplified models of velocity-changing collisions are commonly used to describe Dicke-narrowed profiles. The first, known as the soft-collision model, assumes that a single collision has a negligible influence on absorber motion. This assumption, which enables one to treat the absorber motion as purely diffusional, leads to the Galatry profile (GP) [47]. The soft-collision model is more applicable to the case of a relatively light perturber. Conversely, in the hard-collision model, the post-collision absorber velocity corresponds to a Maxwellian distribution, but does not depend on its velocity before collision. This assumption leads to the Nelkin-Ghatak profile (NGP) [48,49]. Despite the physically unrealistic assumption which underpins this profile, the form of the NGP can be justified by applying the generalized Hess method (GHM) to the line-shape problem [54]. The NGP has been widely used in line-shape analysis because of its simple form. This property of the NGP makes it easy to incorporate speed-dependent effects and gives rise to the speed-dependent Nelkin-Ghatak profile (SDNGP) [49,56]. The simplest realistic model of velocity-changing collisions taking into account the mass ratio of colliding molecules is the rigid-sphere model [31,39]. This model incorporates the relative importance of the speed- and direction-changing collisions [37,57]. A rigid-sphere model of collisions was applied in the billiard-ball profile (BBP) and its speed-dependent version (SDBBP) [31,37].

An additional effect influencing the line shape arises from correlations between velocity-changing and dephasing (state changing) collisions. Rautian and Sobelman [49] gave the correlated NGP (CNGP) profile, which was used by Pine [50] to demonstrate the importance of this effect. The CNGP is equivalent to the line shape obtained on a quantum basis by Demeio *et al.* [54] but the meaning of the parameters in these two profiles is different. In the CNGP profile, the ν_{diff} is replaced by the complex frequency ν_{opt} which generally can be written as $\nu_{\mathrm{opt}}=\nu_{\mathrm{diff}}-\eta_W\Gamma-i\eta_S\Delta$. Here η_W and η_S are correlation parameters which are sometimes assumed to be equal, i.e., $\eta=\eta_W=\eta_S$. The model is called fully correlated when $\eta=1$. A detailed discussion and application of the speed-dependent version of this profile (CSDNGP) has been carried out by Pine [58]. Finally the same modification is applicable to the SDBBP. In this case replacing ν_{diff} by ν_{opt} yields its correlated version CSDBBP. Such profiles were fitted for the first time to experimental data for measurements of CO perturbed by Ar [60,61]. Wehr *et al.* [60,61] clearly demonstrated how inelastic collisions lead to a reduction of Dicke narrowing. A similar situation can be found in atomic systems where dephasing collisions lead to the observable elimination of the Dicke narrowing [59]. Also, a complex ν_{opt} in the CSDBBP has been used to analyze the line shape of HF perturbed by Ar [34,62].

IV. RESULTS AND DISCUSSION

To demonstrate the applicability of our CRDS spectrometer for detailed line-shape investigations we considered the pair of transitions labeled *A* and *B* given in Table I. Transition *B* has a line intensity more than 3000 times weaker than that of transition *A*, although inspection of the HITRAN 2004 line list indicates that it is relatively isolated. For transition *A* we measured the line shapes with three different perturbing gases He, N_2, and SF_6, having a perturber-to-absorber mass ratio of 0.22, 1.56, and 8.11, respectively. This wide range of masses allowed us to observe the influence of not only velocity-changing collisions but also speed-dependent effects. For transition *B* we investigated self- and N_2-broadened line shapes.

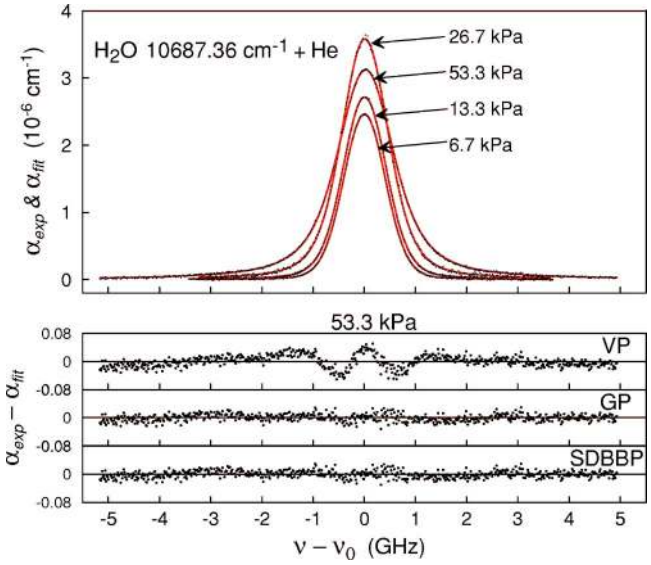

FIG. 2. (Color online) Profiles of H_2O transition A perturbed by He at different pressures with fitted Galatry profiles (upper panel). Residuals for fits (lower panel) of VP, GP, and SDBBP to the $p=53.3$ kPa profile.

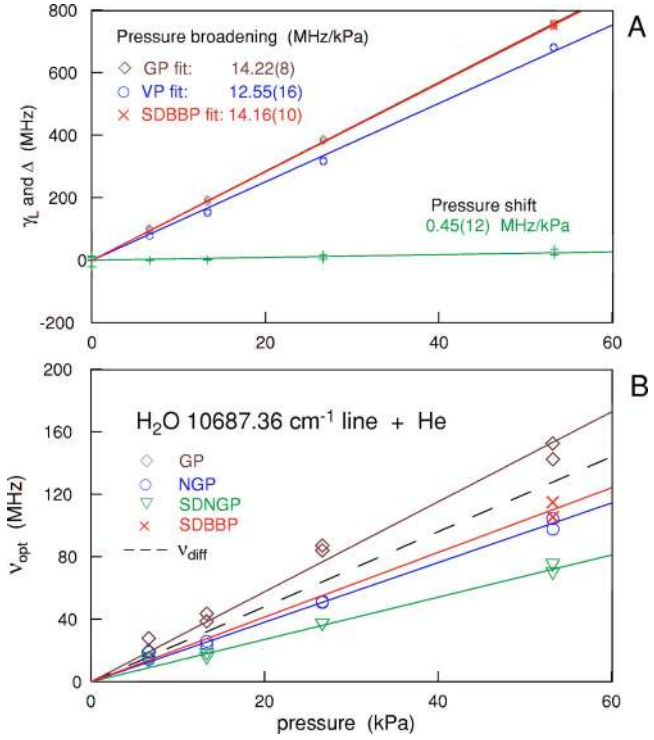

FIG. 3. (Color online) Dependence of fitted Lorentzian width (FWHM) γ_L and shift Δ [graph (A)] and frequency of velocity-changing collisions ν_{opt} [graph (B)] on He pressure p.

The study of rovibrational water vapor line shapes in the presence of various perturbing gases has been an active area of research for many years. Some recent examples of these investigations can be found in Refs. [45,63–71] and in their references.

A. Strong transition

In Fig. 2 we present measured line profiles of transition A perturbed by He at different pressures ranging from 6.7 kPa to 53.3 kPa. Also shown are the Galatry profiles (GP) determined by least-squares fits to the measurements. The residuals of the VP, GP, and SDBBP fits to the highest-pressure profile data are shown at the bottom of the figure. Both profiles have Doppler widths γ_D (FWHM) constrained to the value corresponding to the measured cell temperature. The Lorentzian width $\gamma_L=2\Gamma$ (FWHM) and frequency of velocity-changing collisions ν_{opt} (in the GP) were treated as variable fit parameters. In the SDBBP profile the speed dependence of collisional width and shift were assumed to be given by Eq. (9) with $q=5$. For the lines investigated in this article realistic functions describing the speed dependence of collisional width and collisional shift were not available in the literature. Therefore we were forced to arbitrarily select these functions. Nevertheless, even with this approach we are able to demonstrate the significance of speed-dependent phenomena.

As expected the VP does not reproduce the experimental line shape, in contrast to the GP for which agreement between the observations and model is quite good. Figure 3 shows the dependence of the fitted Lorentzian (collisional) width γ_L and shift Δ [graph (A)] and ν_{opt} [graph (B)] on He pressure p. The pressure-broadening coefficient γ_L/p and pressure shift coefficient Δ/p obtained from linear fits of these dependences are given in Fig. 3(a). For the purpose of comparison we also present results obtained for NGP and SDNGP. It is worth noting that the pressure-broadening coefficients from the VP and GP fits differ by $\simeq 12\%$ which is much more than the combined relative uncertainty of these values (1.3% and 0.6%). The difference between γ_L/p from the GP fit and that from the SDBBP fit is within their standard uncertainties. Moreover, the GP and SDBBP models give a more linear dependence of γ_L on pressure than does the VP. The pressure shift coefficient Δ/p is very small compared to γ_L/p and has a positive sign (blueshift) consistent with previously reported results for molecular and atomic lines perturbed by He [72,73]. The dependence of ν_{opt} on pressure [Fig. 3(b)] is linear and close to the value ν_{diff} (2.4 MHz/kPa [74]) corresponding to the diffusion coefficient of H_2O in He (dashed line). The results presented in Fig. 3(b) clearly demonstrate that the amount of narrowing derived from the data analysis depends significantly on the line-shape model. Moreover, even when the perturber mass is 4.5 times smaller than that of the absorber the speed dependence of Γ can affect the results. Similar observations can be found for CO perturbed by He [75].

The line shape of transition A is more complicated in the case of broadening by nitrogen. Figure 4 presents experimental and fitted profiles of this transition perturbed at different pressures for the N_2-broadening case. The residual plots correspond to the respective fits of the VP, GP, and SDBBP to the measured profile at $p=13.3$ kPa. These results should be analyzed together with Fig. 5(b) in which the dependence of the fitted ν_{opt} on N_2 pressure is presented for the respective line-shape models. Again, as expected, the Voigt profile clearly disagrees with the measured profile and the shape of

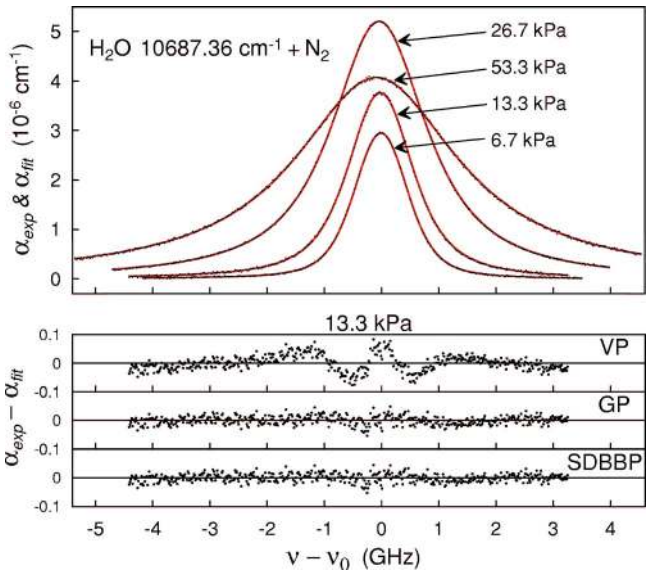

FIG. 4. (Color online) Experimental and fitted profiles of H_2O transition A perturbed by N_2 at different pressures (upper panel). Residuals corresponding to fits (lower panel) of VP, GP, and SDBBP to the $p=13.3$ kPa profile.

the residuals indicates the occurrence of Dicke narrowing. The residuals for the GP are close to zero; however, the fitted values for ν_{opt} depend nonlinearly on pressure. We note that the residuals for the NGP (not shown in Fig. 4) are qualitatively similar to the GP case. Also the ν_{opt} for NGP varies similarly with p [see Fig. 5(b)] as for the GP. Such a nonlinear dependence of ν_{opt} on pressure has been observed in other systems (see, e.g., [76–79]) and is characteristic of lines for which speed-dependent effects cannot be neglected. Two profiles were fitted which take these effects into account: the SDNGP and SDBBP, the latter of which, as described earlier, uses a more realistic model of velocity-changing collisions. For both profiles we used the speed dependence of the collisional width and collisional shift described by Eq. (9) with $q=5$. This q value was also used by Claveau *et al.* to model speed-dependent effects for H_2O lines [80] to give relatively good agreement with experimental data in the absence of better estimates to the interaction potential. The shape of residuals for the SDBBP fit is slightly better than for the GP fit (the same fit quality, not shown here, was obtained for the SDNGP fit), but the fitted ν_{opt} now varies linearly with pressure. The ν_{opt} values for the SDBBP fit are closer to the diffusion coefficient of H_2O in N_2 ($\nu_{\text{diff}}/p=9.0$ MHz/kPa [74]) than for those yielded by the SDNGP fit, but they are still about 40% too small. Such a disagreement was observed for other systems and was attributed to correlation between velocity-changing and dephasing collisions [50,58–61,63,75,76,81].

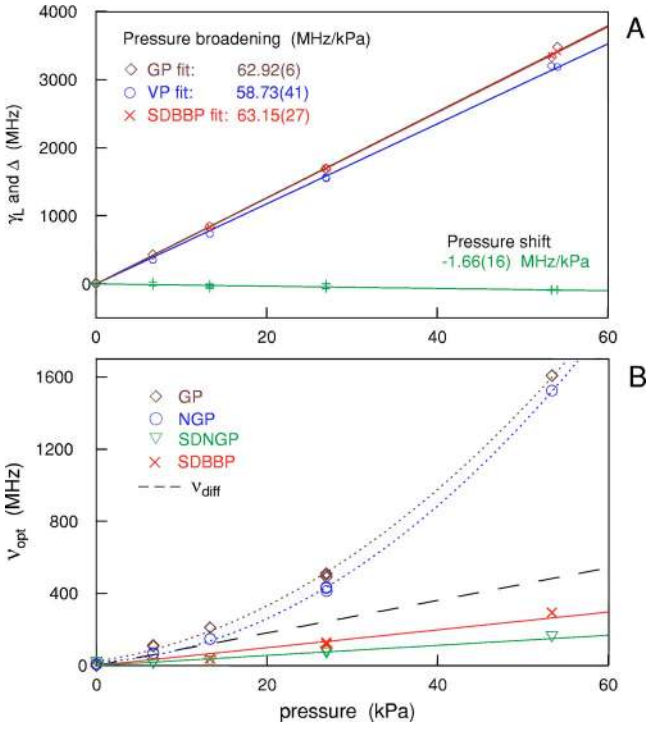

FIG. 5. (Color online) Dependence of fitted Lorentzian width (FWHM) γ_L and shift Δ [graph (A)] and frequency of velocity-changing collisions ν_{opt} [graph (B)] on N_2 pressure p for different theoretical profiles.

In Fig. 5(a) the collisional width and collisional shift of transition A are presented as a function of N_2 pressure. Values of the pressure broadening coefficients γ_L/p for the various line-shape models and the pressure-shift coefficient Δ/p are reported. As expected the best linearity of γ_L with pressure was achieved for the SDBBP and SDNGP fits for which the relative uncertainty of γ_L/p was also the smallest (0.1%). The results obtained for the SDNGP are not shown in Fig. 5(a) because they are indistinguishable from those of the SDBBP. However, γ_L/p from the GP fit differs by 0.4%. This is not surprising since line narrowing (which can result from speed-dependent effects as well as Dicke narrowing) can be well modeled by overestimation of the Dicke narrowing which can occur when a GP is fit to a measured line shape that exhibits speed dependence [82–84].

In the case of SF_6 as a perturber the speed-dependent effects were expected to be much stronger than for N_2 because of the relatively high mass of the SF_6. In Fig. 6 we present experimental profiles of transition A broadened by SF_6 at different pressures. Also shown are the residuals for fits of the theoretical profiles to the data for the case $p=26.7$ kPa. Strong line asymmetry can be seen in the first two residual plots corresponding to the symmetrical profiles (VP, BBP). This asymmetry can be explained by speed-dependent effects together with the relatively large pressure-shift coefficient which is presented in Fig. 7. Nevertheless, one should remember that such asymmetry can be a result of the simultaneous effect of the speed dependence of the collisional shift, and the correlation between velocity-changing and dephasing collisions, line mixing, and collision-time asymmetry [34,52,81]. For the case of SF_6 as the perturber, we started our analysis in the same way as was done for the He and N_2 cases by assuming the same speed dependence for the width and shift and letting $q=5$. However, this approach yielded a negative value for the real part of the fit-derived narrowing parameter. Since we did not have any realistic theoretical prediction for the speed dependence, we arbitrarily assumed no speed dependence for the width. For the

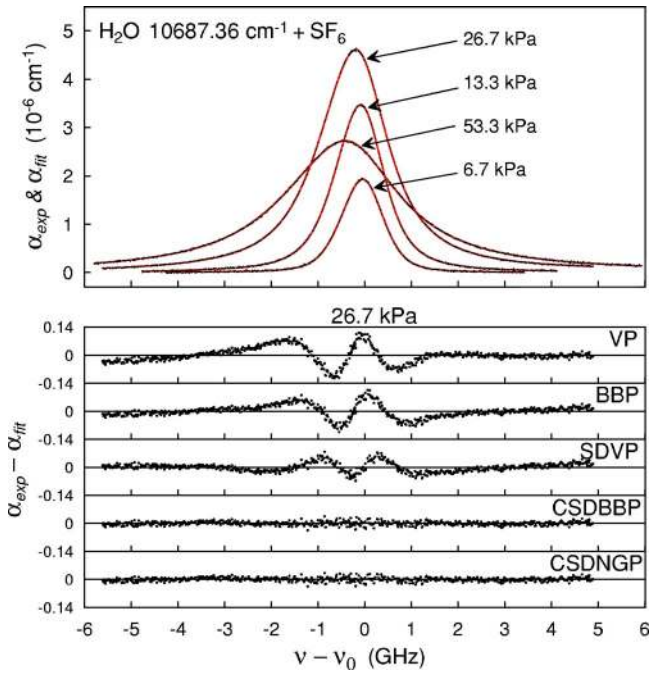

FIG. 6. (Color online) Experimental and theoretical profiles of H_2O transition A perturbed by SF_6 at different pressures (upper panel). Residuals for fits of theoretical profiles (lower panel) to the $p=26.7$ kPa data.

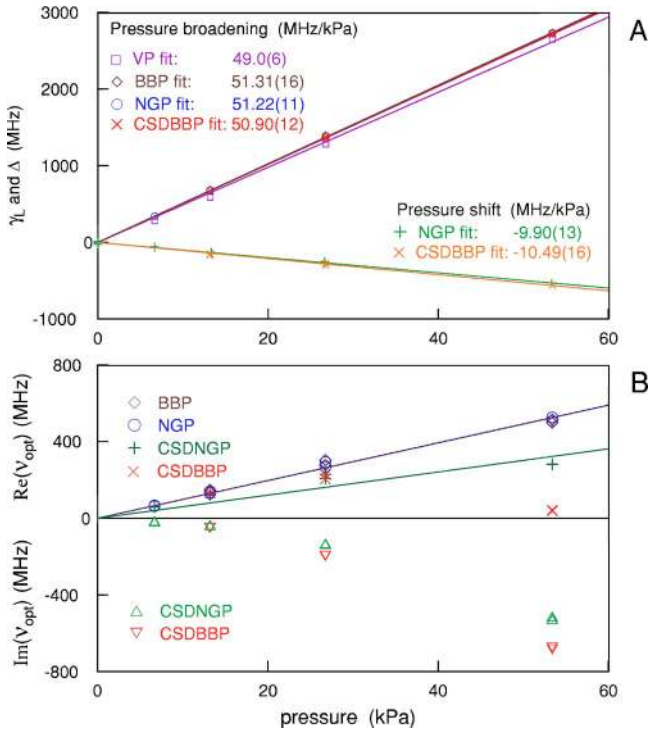

FIG. 7. (Color online) Dependence of fitted Lorentzian width (FWHM) γ_L and shift Δ [graph (A)] and frequency of velocity-changing collisions ν_{opt} [graph (B)] on SF_6 pressure p for different theoretical profiles.

shift we assumed a speed dependence given by Eq. (9) with $q=6$. Our intent was to demonstrate properties of the experimental results as well as to emphasize theoretical needs. Indeed the observed line asymmetry can be modeled by the SDVP when $q=6$ for the shift is assumed. This profile gives residuals which are symmetrical around the line center but which are still far from a perfect fit to the measurements. A better quality of fit can be obtained using either the CSDBBP or CSDNGP as can be seen in Fig. 6. The real part of the fitted values of ν_{opt} for the NGP, BBP, CSDNGP, and CSDBBP profiles and the imaginary part of ν_{opt} for the CSDNGP and CSDBBP profiles are presented in Fig. 7(b). It should be emphasized that more realistic models for the speed dependence of the collisional width and collisional shift are required in order to draw any conclusions about the narrowing of this line in the presence of SF_6.

With regard to the measurements of water vapor transition A perturbed by SF_6, comparison of the various pressure-broadening coefficients derived from the fits to theoretical profiles indicates that the γ_L/p coefficient can differ by about 1% from the CSDBBP value when speed-dependent effects (BBP and NGP) are neglected. These differences are more than the relative standard uncertainty of γ_L/p (less then 0.3%) and can represent the biggest contribution to systematic error in the determination of the broadening coefficient. In Fig. 7(a) we also present the influence of the line profile on the determined pressure-shift coefficient. As a consequence of the relatively pronounced line asymmetry, the pressure-broadening coefficients Δ/p determined from fits of the BBP or other symmetrical profiles differ by over 5% from that determined by the CSDBBP fit.

The pressure-broadening γ_L/p and pressure-shift Δ/p coefficients for water vapor transition A perturbed by He, N_2, and SF_6, obtained using the theoretical profiles that best fit to experimental data, are summarized in Table II.

We investigated the sensitivity of the fitted line area $\mathcal{A}$ to the choice of theoretical line shape for transition A. The line area can be defined as the integral $\mathcal{A}=\int d\nu\alpha(\nu)$ of the absorption coefficient $\alpha(\nu)$ over the radiation frequency ν. The line area $\mathcal{A}=NS$ is proportional to the line intensity S and absorber concentration N. The relatively complicated line shape associated with SF_6 as the perturber makes it an interesting example to quantify this effect. In Fig. 8 we present the relative deviation of the line area as a function of perturber pressure determined from the fits of the various model profiles to the same data. The deviation given in Fig. 8 is the relative difference with respect to the value obtained from the CSDNGP fit. We chose this profile as a reference because

TABLE II. Pressure-broadening coefficient γ_L/p and pressure shift coefficient Δ/p of H_2O lines perturbed by different gases. All results were obtained from fitting the SDBBP model to the data except for the SF_6-broadened line A (CSDBBP fit) and self-broadened line B (NGP fit).

Transition	Perturber	γ_L/p [MHz/kPa]	Δ/p [MHz/kPa]
A	He	14.16(10)	0.45(12)
A	N_2	62.92(6)	−1.66(16)
A	SF_6	50.90(12)	−10.49(16)
B	H_2O	275.3(1.1)	−30.1(1.0)
B	N_2	61.1(8)	−3.37(11)

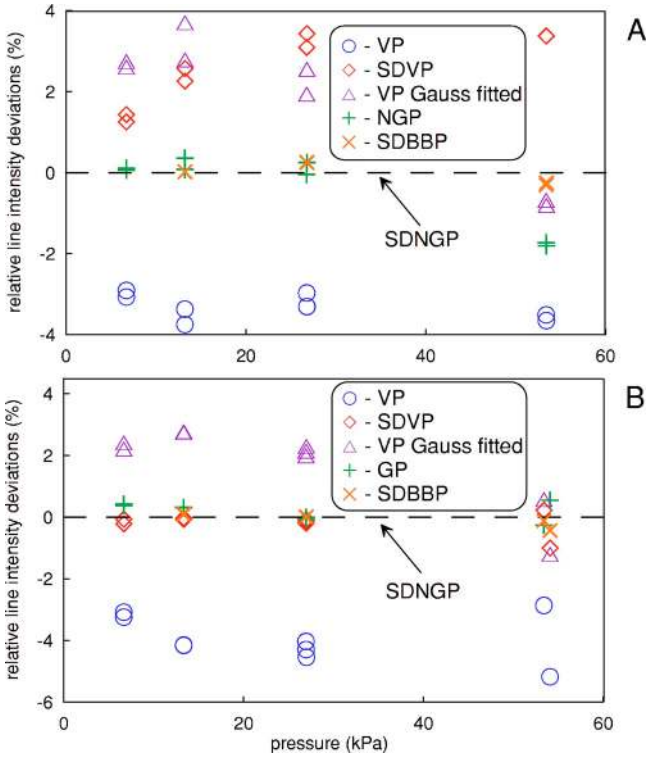

FIG. 8. (Color online) Relative deviation of the line area determined from fits of model profiles to experimental data for the H_2O transition A perturbed by SF_6 [graph (A)] and by N_2 [graph (B)] at different pressures. The reference model is the SDNGP.

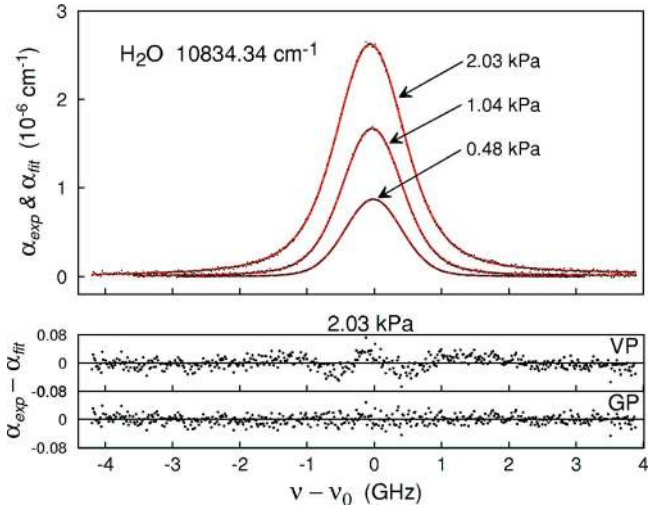

FIG. 9. (Color online) Experimental profiles of transition B and associated residuals for VP and GP fits to the data. Sample conditions correspond to $p=2$ kPa of pure H_2O.

it gave a good fit with residuals uniformly spread around zero. We note that although the same quality in the fit residuals was achieved for the CSDBBP profile, the CSDBBP was not fitted to the lowest-pressure data because of numerical difficulties that prevent convergence of the model calculations. This lack of convergence of the CSDBBP results when the pressure width is smaller than about one-half of the Doppler width [37]. As can be seen the commonly used VP with the Doppler width constrained to the theoretical value corresponding to the gas temperature leads to a systematic underestimate of the area of about 4%. The same was found before by Ponsardin and Browell [64] for air-broadened water lines. Interestingly, the fitted VP yields a 3% overestimate of the area for low pressure when using an unconstrained Doppler width. For higher pressure the fitted VP gives improved estimates of the line area. The NGP gives a good area estimation for low pressures but not for high pressure where a 2% underestimation is observed. As expected the CSDBBP leads to almost the same line areas as the reference case CSDNGP. For N_2 as a perturber [Fig. 8(b)] a very similar dependence of the fitted line area on pressure was observed for the VP with Doppler width constrained ($\approx$4% underestimation) and fitted ($>$2% overestimation for low pressure). However, profiles taking Dicke-narrowing or speed-dependent effects (or both) gave line-area deviations less than 0.5%. These results show that errors associated with inappropriate line shapes (specifically for the transition under investigation and probably for other transitions) can introduce non-negligible systematic uncertainty in the measurement of line intensity based on the fitting of measured absorption spectra. We also investigated the influence of the spectral range of the scan on the line-intensity determination. After numerical simulations we found that by increasing the spectral range from 10 GHz to 40 GHz deviations in the fitted areas associated with the different profiles were reduced approximately twofold. Finally we note that any number of profiles which give the same quality of fit to the data can have residuals that are dominated by the random noise in the measurements. From the point of view of line-intensity determination, all such profiles are essentially indistinguishable and will yield the same line intensity within their combined respective fit uncertainties. This set of best-fit profiles may include those with a rigorous physical basis as well as those which are not physically well justified such as those with fitted parameters having poor physical meaning.

B. Weak transition

Measurements of profiles of the relatively weak transition B with high SNR required higher pressures of water vapor (about 0.5–2 kPa). These conditions allowed us to determine the self-broadening and pressure shift as well as the line intensity with low uncertainty. In Fig. 9 we present experimental profiles of transition B and associated residuals for the VP and GP fits to the highest-pressure data. As can be seen, the profile is symmetrical and indicates Dicke narrowing. We do not observe any signs of speed dependence of collisional broadening and shifting which could be understood in terms of the dipole-dipole interaction between water molecules with $q=3$. The GP (and the NGP which is not shown here) agrees well with the experimental profile over the pressure range investigated. In Fig. 10 the self-broadening γ_L, the pressure shift Δ, and ν_{opt} characterizing Dicke narrowing for transition B are shown as a function of pressure. There is a big difference in the pressure-broadening coefficient γ_L/p obtained using profiles with and without Dicke narrowing taken into account. The VP underestimates

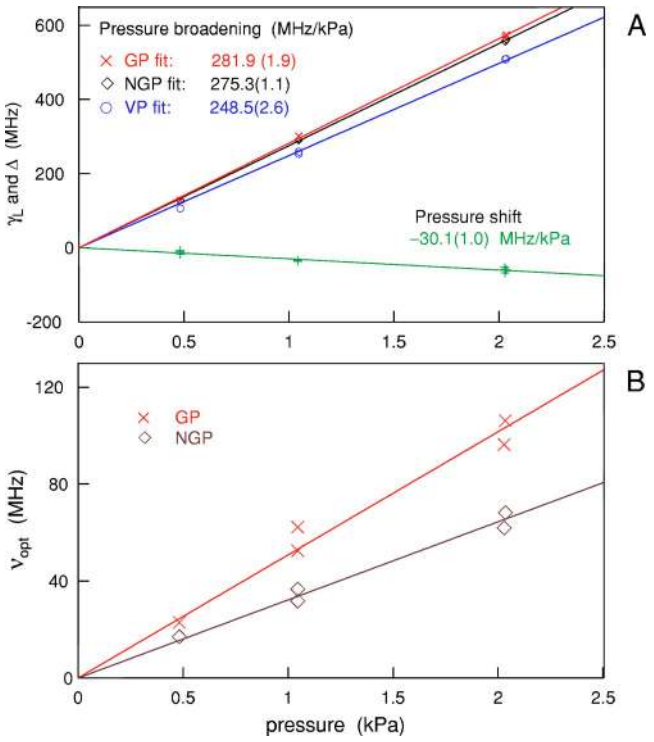

FIG. 10. (Color online) Dependence of the self-broadening γ_L, shift Δ, and ν_{opt} characterizing Dicke narrowing on pressure for transition B obtained from the fits of different profiles to the experimental data.

γ_L/p by over 13%, and the difference between γ_L/p determined from the GP and NGP is 2.4% which is within three standard combined uncertainties of these values. The fitted values of ν_{opt} depend linearly on pressure for both the GP and NGP profiles. However, we did not estimate the diffusion coefficient of H_2O molecule in H_2O to calculate the quantity ν_{diff}.

In Fig. 11 the fitted area $\mathcal{A}$ of transition B is plotted against H_2O concentration N for the VP, GP, and NGP fits.

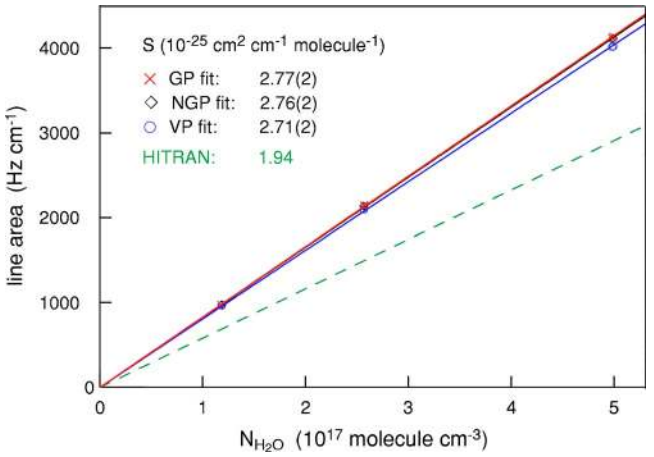

FIG. 11. (Color online) Area $\mathcal{A}$ of transition B is plotted against the H_2O concentration N for the VP, GP, and NGP fits. The dashed line corresponds to the HITRAN 2004 value of line intensity evaluated at $T=296$ K.

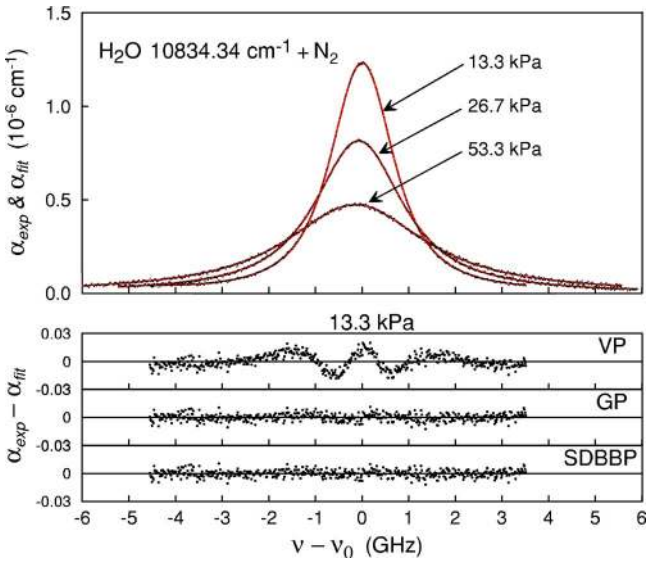

FIG. 12. (Color online) Experimental and theoretical profiles of transition B perturbed by N_2 at different pressures and residuals for fits of theoretical profiles to the $p=13.3$ kPa spectrum.

The line intensities S calculated from a linear dependence of $\mathcal{A}$ on N are also indicated. The dashed line corresponds to the HITRAN 2004 [24] value equal to $S=1.94\times10^{-25}$ cm^2 cm^{-1} molecule^{-1}. The measured line intensity $S=2.77(2)\times10^{-25}$ cm^2 cm^{-1} molecule^{-1} differs significantly (43%) from the room-temperature value reported in HITRAN 2004 while the relative standard uncertainty of our result is only 0.7%. This result indicates the possibility of large uncertainty in reported line intensities for relatively weak H_2O lines. Using an oversimplified line profile such as the VP leads to an underestimate of $\simeq2\%$ for the intensity of investigated line. The GP and NGP give very similar line-intensity values which is not surprising since they both fit the measured spectrum perfectly to within the random noise in our experiment.

The line shape of transition B was also measured in the case of N_2 as the perturber. For this weak line it was more complicated than for transition A because a relatively high pressure (1.3 kPa) of H_2O was required to achieve a good SNR in the CRDS spectrum. We observed that the self-broadening and self-shift could not be neglected in the determination of the N_2-broadening γ_L/p and -shift Δ/p coefficients. The experimental line shapes are presented in Fig. 12 for different N_2 pressures, and the residuals are shown corresponding to fits of the theoretical profiles to the $p=13.3$ kPa spectrum. The line narrowing can be quite well modeled by GP (NGP and BBP give similar results); however, there remains a small asymmetry in the GP residuals. As shown in residuals of the SDBBP, the fit quality can be improved by taking speed-dependent effects into account. Here we show the case where the speed dependence of γ_L and Δ was calculated using Eq. (9) in which $q=5$. However, the same quality of fit was also achieved for $q=4$ and $q=6$.

In Fig. 13 we present the collisional width and collisional shift of transition B [graph (A)] and the frequency of velocity-changing collisions ν_{opt} [graph (B)] obtained from

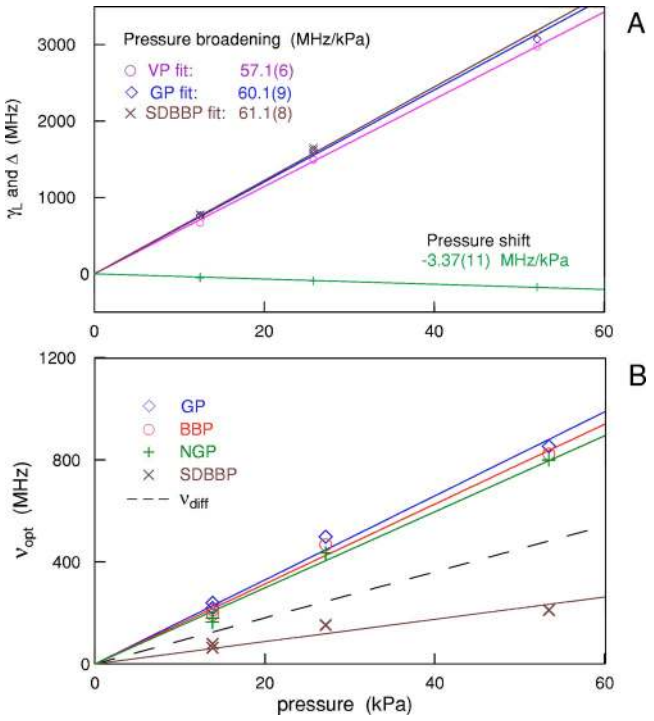

FIG. 13. (Color online) Dependence of the fitted Lorentzian width (FWHM) γ_L and shift Δ [graph (A)] and frequency of velocity-changing collisions ν_{opt} [graph (B)] of transition B on the N_2 pressure p for different theoretical profiles.

fits of the respective profiles to the experimental data. The ν_{opt} parameter increases linearly with pressure for all profiles considered which take Dicke narrowing into account. Furthermore, as was observed for transition A, neglecting speed-dependent effects leads to an overestimation of ν_{opt} as compared to ν_{diff} calculated from the diffusion coefficient of H_2O in N_2. The SDBBP gives values of ν_{opt} that are much lower then ν_{diff}.

Note that in the pressure width γ_L and shift Δ parameters presented in Fig. 13(a) the self-broadening and self-shift for transition B were subtracted. The effect of the line-shape model on γ_L is seen. Compared to the SDBBP which gives the best agreement with experimental profiles, the VP underestimates the pressure-broadening coefficient by about 6% while the GP (NGP and BBP) yields values that are approximately 1.5% low.

Values of self- and N_2-broadening and shift coefficients calculated from fits of profiles which best agree with the experimental spectra are given in Table II.

V. CONCLUSION

We have demonstrated that frequency-stabilized CRDS is amenable to a careful analysis of the physical effects that determine the shape of spectral lines. Probing infrared absorption transitions of H_2O, we have carried out the first verification involving CRDS of several line-shape models. Our investigation leads us to conclude that progress in understanding the effects which determine the shape of water lines will require knowledge of realistic and physically motivated functions that describe the speed dependence of collisional broadening and collisional shifting.

We emphasize that unlike Fourier transform spectroscopy and other high-sensitivity absorption methods such as photoacoustic spectroscopy or techniques based on narrowband cw lasers, the single-mode frequency-stabilized CRDS approach, as implemented here, is relatively free of confounding instrumental effects that typically cause spectral distortions at the MHz frequency level. Further, CRDS offers much higher sensitivity than ordinary laser absorption spectroscopy methods, many of which use single-mode lasers and frequency doubling or difference frequency generation (DFG) schemes for wavelength conversion to relevant spectral regions. The relatively high sensitivity of CRDS is especially important in the case of weak absorption lines which could not be investigated with adequate signal-to-noise ratio using most other spectroscopic methods.

We have shown that differences in the line intensities determined by fitting various line-shape models to the same high-resolution absorption spectra (corresponding to self- and foreign-broadened H_2O) can be significant, varying in some cases by more than a few percent. These results illustrate the difficulty in assigning relative uncertainties in measured line intensities at the subpercent level, especially for conditions in which collisional narrowing and speed-dependent effects occur. Importantly, line-shape effects may be distorted, masked, or unobserved when using experimental methods that have insufficient spectral resolution and/or low signal-to-noise ratio. Similarly, these effects are expected to influence measurements of pressure-broadening coefficients and pressure-shift coefficients as well as absorber concentration and temperature. Consequently minimizing the uncertainty of these measurements will require the sensitivity, linearity, and spectral resolution to distinguish and select appropriate line-shape models used for data analysis.

ACKNOWLEDGMENTS

The authors would like to thank Dr. Keith A. Gillis and Dr. Alan S. Pine for carefully reading the manuscript and offering helpful suggestions. Finally, we acknowledge the contributions of the NIST Advanced Technology Program and the NIST Office of Microelectronics Programs which provided financial support.

[1] P. M. Sinclair, J. Ph. Berger, X. Michaut, R. Saint-Loup, R. Chaux, H. Berger, J. Bonamy, and D. Robert, Phys. Rev. A **54**, 402 (1996).

[2] N. S. Higdon, E. V. Browell, P. Ponsardin, B. E. Grossmann, C. F. Butler, T. H. Chyba, M. N. Mayo, R. J. Allen, A. W. Heuser, W. B. Grant, S. Ismail, S. D. Mayor, and A. F. Carter, Appl. Opt. **33**, 6422 (1994).

[3] C. Boulet, C. R. Phys. **5**, 201 (2004).

[4] W. Gurlit, R. Zimmermann, C. Giesemann, T. Fernholz, V. Ebert, J. Wolfrum, U. Platt, and J. P. Burrows, Appl. Opt. **44**, 91 (2005).
[5] C. E. Miller, L. R. Brown, R. A. Toth, D. C. Benner, and V. M. Devi, C. R. Phys. **6**, 876 (2005).
[6] J. Hussong, W. Stricker, X. Bruet, P. Joubert, J. Bonamy, D. Robert, X. Michaut, T. Gabard, and H. Berger, Appl. Phys. B: Lasers Opt. **70**, 447 (2000).
[7] R. Wehr, E. McKernan, A. Vitcu, R. Ciuryło, and J. R. Drummond, Appl. Opt. **42**, 6595 (2003).
[8] E. Jourdanneau, F. Chaussard, R. Saint-Loup, T. Gabard, and H. Berger, J. Mol. Spectrosc. **233**, 219 (2005).
[9] X. Zhou, J. B. Jeffries, and R. K. Hanson, Appl. Phys. B: Lasers Opt. **81**, 711 (2005).
[10] A. S. Pine, J. Quant. Spectrosc. Radiat. Transf. **57**, 145 (1997).
[11] G. D. Sheldon, P. M. Sinclair, M. P. Le Flohic, J. R. Drummond, and A. D. May, J. Mol. Spectrosc. **192**, 406 (1998).
[12] C. Boulet, P.-M. Flaud, and J.-M. Hartmanna, J. Chem. Phys. **120**, 11053 (2004).
[13] K. K. Lehmann and D. Romanini, J. Chem. Phys. **105**, 10263 (1996).
[14] J. T. Hodges, J. P. Looney, and R. D. van Zee, J. Chem. Phys. **105**, 10278 (1996).
[15] J. T. Hodges, J. P. Looney, and R. D. van Zee, Appl. Opt. **35**, 4112 (1996).
[16] D. Romanini, A. A. Kachanov, N. Sadeghi, and F. Stoeckel, Chem. Phys. Lett. **264**, 316 (1997).
[17] D. Romanini, A. A. Kachanov, and F. Stoeckel, Chem. Phys. Lett. **270**, 538 (1997).
[18] J. B. Dudek, P. B. Tarsa, A. Velasquez, M. Wladyslawski, P. Rabinowitz, and K. K. Lehmann, Analy. Chem. Appl. Opt. **75**, 4499 (2003).
[19] A. R. Awtry and J. H. Miller, Appl. Phys. B: Lasers Opt. **75**, 255 (2002).
[20] M. Hippler and M. Quack, J. Chem. Phys. **116**, 6045 (2002).
[21] P. Macko, D. Romanini, S. N. Mikhailenko, O. V. Naumenko, S. Kassi, A. Jenourvrier, Vl. G. Tyuterev, and A. Campargue, J. Mol. Spectrosc. **227**, 90 (2004).
[22] J. T. Hodges, H. P. Layer, W. W. Miller, and G. E. Scace, Rev. Sci. Instrum. **75**, 849 (2004).
[23] J. T. Hodges and R. Ciuryło, Rev. Sci. Instrum. **76**, 023112 (2005).
[24] L. S. Rothman *et al.*, J. Quant. Spectrosc. Radiat. Transf. **96**, 139 (2004).
[25] D. Romanini, P. Dupre, and R. Jost, Vib. Spectrosc. **19**, 93 (1999).
[26] C. R. Bucher, K. K. Lehmann, D. F. Plusquellic, and G. T. Fraser, Appl. Opt. **39**, 3154 (2000).
[27] E. W. Smith, J. Cooper, W. R. Chappell, and T. Dillon, J. Quant. Spectrosc. Radiat. Transf. **11**, 1547 (1971); **11**, 1567 (1971).
[28] V. A. Alekseev, T. L. Andreeva, and I. I. Sobelman, Zh. Eksp. Teor. Fiz. **62**, 614 (1972).
[29] G. Nienhuis, J. Quant. Spectrosc. Radiat. Transf. **20**, 275 (1978).
[30] P. R. Berman, in *New Trends in Atomic Physics*, edited by G. Grynberg and R. Stora Les Houches Lectures, Session XXX-VIII, (North-Holland, Amsterdam, 1982), Vol. 1, p. 451.
[31] R. Blackmore, J. Chem. Phys. **87**, 791 (1987).
[32] R. Blackmore, S. Green, and L. Monchik, J. Chem. Phys. **91**, 3846 (1989).
[33] B. Lance and D. Robert, J. Chem. Phys. **111**, 789 (1999).
[34] A. S. Pine and R. Ciuryło, J. Mol. Spectrosc. **208**, 180 (2001).
[35] D. A. Shapiro, R. Ciuryło, R. Jaworski, and A. D. May, Can. J. Phys. **79**, 1209 (2001).
[36] P. Joubert, P. N. M. Hoang, L. Bonamy, and D. Robert, Phys. Rev. A **66**, 042508 (2002).
[37] R. Ciuryło, D. A. Shapiro, J. R. Drummond, and A. D. May, Phys. Rev. A **65**, 012502 (2002).
[38] L. Bonamy, H. Tran Thi Ngoc, P. Jouberta, and D. Robert, Eur. Phys. J. D **31**, 459 (2004).
[39] M. J. Lindenfeld, J. Chem. Phys. **73**, 5817 (1980).
[40] D. A. Shapiro, R. Ciuryło, J. R. Drummond, and A. D. May, Phys. Rev. A **65**, 012501 (2002).
[41] P. R. Berman, J. Quant. Spectrosc. Radiat. Transf. **12**, 1331 (1972).
[42] J. Ward, J. Cooper, and E. W. Smith, J. Quant. Spectrosc. Radiat. Transf. **14**, 555 (1974).
[43] S. Green and J. M. Hutson, J. Chem. Phys. **100**, 891 (1994).
[44] J.-M. Hartmann and C. Boulet, J. Chem. Phys. **113**, 9000 (2000).
[45] R. R. Gamache and J.-M. Hartmann, J. Quant. Spectrosc. Radiat. Transf. **83**, 119 (2004).
[46] S. Chandrasekhar, Rev. Mod. Phys. **15**, 1 (1943).
[47] L. Galatry, Phys. Rev. **122**, 1218 (1961).
[48] M. Nelkin and A. Ghatak, Phys. Rev. **135**, A4 (1964).
[49] S. G. Rautian and I. I. Sobelman, Usp. Fiz. Nauk **90**, 209 (1966) [Sov. Phys. Usp. **9**, 701 (1967)].
[50] A. S. Pine, J. Chem. Phys. **101**, 3444 (1994).
[51] P. Joubert, R. Bonamy, D. Robert, J.-L. Domenech, and D. Bermejo, J. Quant. Spectrosc. Radiat. Transf. **61**, 519 (1999).
[52] R. Ciuryło, A. S. Pine, and J. Szudy, J. Quant. Spectrosc. Radiat. Transf. **68**, 257 (2001).
[53] J. P. Looney, Ph.D. thesis, The Pennsylvania State University (1987).
[54] L. Demeio, S. Green, and L. Monchik, J. Chem. Phys. **102**, 9160 (1995).
[55] R. M. Herman, in *Spectral Line Shapes*, edited by J. Seidel (AIP, Melville, NY, 2001), p. 237.
[56] B. Lance, G. Blanquet, J. Walrand, and J.-P. Bouanich, J. Mol. Spectrosc. **185**, 262 (1997).
[57] R. Ciuryło, D. Lisak, and J. Szudy, Phys. Rev. A **66**, 032701 (2002).
[58] A. S. Pine, J. Quant. Spectrosc. Radiat. Transf. **62**, 397 (1999).
[59] D. Lisak, A. Bielski, R. Ciuryło, J. Domysławska, R. S. Trawiński, and J. Szudy, J. Phys. B **36**, 3985 (2003).
[60] R. Wehr, A. Vitcu, R. Ciuryło, F. Thibault, J. R. Drummond, and A. D. May, Phys. Rev. A **66**, 062502 (2002).
[61] R. Wehr, R. Ciuryło, A. Vitcu, F. Thibault, J. R. Drummond, and A. D. May, J. Mol. Spectrosc. (to be published).
[62] R. Ciuryło, A. Bielski, J. R. Drummond, D. Lisak, A. D. May, A. S. Pine, D. A. Shapiro, J. Szudy, and R. S. Trawiński, in *Spectral Line Shapes*, edited by C. A. Back (AIP, Melville, NY, 2002), p. 151.
[63] B. E. Grossmann and E. V. Browell, J. Quant. Spectrosc. Radiat. Transf. **45**, 339 (1991).
[64] P. L. Ponsardin and E. V. Browell, J. Mol. Spectrosc. **185**, 58 (1997).
[65] A. Bruno, G. Pesce, G. Rusciano, and A. Sasso, J. Mol. Spectrosc. **215**, 244 (2002).

[66] M.-F. Mérienne, A. Jenouvrier, C. Hermans, A. C. Vandaele, M. Carleer, C. Clerbaux, P.-F. Coheur, R. Colin, S. Fally, and M. Bach, J. Quant. Spectrosc. Radiat. Transf. **82**, 99 (2003).
[67] R. Phelan, M. Lynch, J. F. Donegan, and V. Weldon, Appl. Opt. **42**, 4968 (2003).
[68] A. D. Bykov, N. N. Lavrentieva, V. N. Saveliev, L. N. Sinitsa, C. Camy-Peyret, Ch. Claveau, and A. Valentin, J. Mol. Spectrosc. **224**, 164 (2004).
[69] V. Zeninari, B. Parvitte, D. Courtois, N. N. Lavrentieva, Yu. N. Ponomarev, and G. Durry, Mol. Phys. **102**, 1697 (2004).
[70] L. R. Brown, D. C. Benner, V. M. Devi, M. A. H. Smith, R. A. Toth, J. Mol. Spectrosc. **742**, 111 (2005).
[71] R. A. Toth, J. Quant. Spectrosc. Radiat. Transf. **94**, 1 (2005); **94**, 51 (2005).
[72] A. Henry, D. Hurtmans, M. Margottin-Maclou, and A. Valentin, J. Quant. Spectrosc. Radiat. Transf. **56**, 647 (1996).
[73] M. V. Romalis, E. Miron, and G. D. Cates, Phys. Rev. A **56**, 4569 (1997).
[74] C. Claveau, A. Henry, D. Hurtmans, and A. Valentin, J. Quant. Spectrosc. Radiat. Transf. **68**, 273 (2001).
[75] P. Duggan, P. M. Sinclair, R. Berman, A. D. May, and J. R. Drummond, J. Mol. Spectrosc. **186**, 90 (1997).
[76] D. Lisak, G. Rusciano, and A. Sasso, J. Mol. Spectrosc. **277**, 162 (2004).
[77] P. Duggan, P. M. Sinclair, A. D. May, and J. R. Drummond, Phys. Rev. A **51**, 218 (1995).
[78] J. F. D'Eu, B. Lemoine, and F. Rohart, J. Mol. Spectrosc. **212**, 96 (2002).
[79] D. Lisak, G. Rusciano, and A. Sasso, Phys. Rev. A **72**, 012503 (2005).
[80] C. Claveau, A. Henry, M. Lepère, A. Valentin, and D. Hurtmans, J. Mol. Spectrosc. **212**, 171 (2002).
[81] J. W. Brault, L. R. Brown, C. Chackerian, Jr., R. Freedman, A. Predoi-Cross, and A. S. Pine, J. Mol. Spectrosc. **222**, 220 (2003).
[82] D. Priem, F. Rohart, J. M. Colmont, G. Wlodarczak, and J. P. Bouanich, J. Mol. Spectrosc. **517**, 435 (2000).
[83] D. Priem, J. M. Colmont, F. Rohart, G. Wlodarczak, and R. R. Gamache, J. Mol. Spectrosc. **204**, 204 (2000).
[84] J. M. Colmont, J. F. D'Eu, F. Rohart, G. Wlodarczak, and J. Buldyreva, J. Mol. Spectrosc. **208**, 197 (2001).